SARS-CoV-2 spike antibodies cross-react with dengue virus and enhance infection *in vitro* and *in vivo*

Kamini Jakhar[1†], Sudipta Sonar[1†], Gagandeep Singh[2], Tejeswara Rao Asuru[3†], Garima Joshi[3†], Nisha Beniwal[1], Tania Sarkar[1], Mahima Tiwari[1], Jaskaran Kaur[1], Deepak Kumar Rathore[4], Banwari Lal[1], Sandeep Kumar[1], Puneet Srivastav[1], Satendra Kumar[1], Vikas Phagna[1], Sushma[1], Lokesh Kumar[1], Vishal Gupta[1,5], Pallavi Kshetrapal[6], Savita Singh[6], Nitya Wadhwa[6], Ramachandran Thiruvengadam[6,7], Sreevatsan Raghavan[6], Mudita Gosain[6], Tripti Shrivastava[1], Sankar Bhattacharyya[1], Shailendra Asthana[2], Prasenjit Guchhait[3] and Shailendra Mani[1*]

† Contributed equally

*Corresponding author

Corresponding author: Shailendra Mani, PhD.

Email: shailendramani@thsti.res.in

Author affiliations:

1. Centre for Virus Research, Therapeutics and Vaccines, Translational Health Science and Technology Institute, Faridabad, Haryana, India-120001
2. Computational Biophysics and CADD group, Computational and Mathematical Biology Centre (CMBC), Translational Health Science and Technology Institute (THSTI), Faridabad, Haryana, India-120001
3. Molecular Medicine, Regional Centre for Biotechnology, Faridabad, Haryana, India-120001
4. Centre for Immunobiology and Immunotherapy, Translational Health Science and Technology Institute, Faridabad, Haryana, India-120001

5. Translational Health Science and Technology Institute, Faridabad, Haryana, India-120001
6. Centre for Maternal and Child Health, Translational Health Science and Technology Institute, Faridabad, Haryana, India-120001
7. Department of Biochemistry, Pondicherry Institute of Medical Sciences, Kalathumettupathai, Ganapathichettikulam Village No.20, Kalapet, Puducherry, India-605014.

Abstract:

The presence of non-neutralizing antibodies of any dengue serotype, increase the severity of subsequent infection by other dengue serotypes. During SARS-CoV-2 pandemic, the number of symptomatic dengue cases increased in India. The cross-reactivity of dengue with SARS-CoV-2 is well reported. We investigated the potential of SARS-CoV-2 spike antibodies to modulate dengue infection. *In silico* and *In vitro* studies revealed protein-protein interactions between the spike antibodies and the dengue virus 2 envelope protein. Convalescent plasma from COVID-19 patients and SARS-CoV-2 monoclonal/polyclonal antibodies showed cross-reactivity and impact on dengue infection in cell-based assays. Furthermore, increased dengue viral load was observed in serum, liver, and spleen of mice coinfected with dengue and SARS-CoV-2, compared to only dengue infected animals. Collectively, we demonstrate that SARS-CoV-2 spike antibodies can cross-react with and enhance dengue infectivity. These findings have significant implications for SARS-CoV-2 monitoring and patient management in dengue-endemic regions.

Keywords: SARS-CoV-2; Dengue Virus; Cross-reactivity; Antibody-Dependent Enhancement; AG129 Mice model

52 **Introduction**

53 Dengue is endemic to more than 120 countries with Asia contributing 70% of the global burden
54 (1). Dengue virus (DENV) circulates as four serotypes (DENV 1-4) each containing multiple
55 distinct genotypes. DENV infection can cause mild fever or lead to severe forms like Dengue
56 Haemorrhagic Fever (DHF) and Dengue Shock Syndrome (DSS). Primary infection provides
57 lifelong immunity to homotypic secondary infection but gives partial immunity from
58 heterotypic challenge. Heterotypic secondary infections present with severe symptoms, due to
59 higher viremia catalyzed by Antibody-dependent Enhancement (ADE). Sub-neutralizing
60 antibodies that bind to heterotypic DENV promote FcR-mediated viral entry into cells (2). A
61 stable attachment to Fc receptors by these antibodies, without reaching the neutralization
62 threshold leads to ADE (3).

63 The dynamics of DENV infections during the SARS-CoV-2 pandemic vary globally. A 16%
64 decline in dengue incidences was reported in 2020-21 compared to pre-COVID-19 (4).
65 However, S. Khan *et. al.* revealed a substantial surge in dengue cases in 2021 in specific South
66 Asian countries, including India (~3-fold), Pakistan (>7-fold), and Bangladesh (>19-fold). This
67 contrasted with a noteworthy decline of about 36% across Southeast Asia and Latin America
68 (5). Several regional, environmental, and pandemic-related elements have been reported to
69 shape these intricate dynamics. Disruptions in routine mosquito vector surveillance and control
70 programs during COVID-19 lockdowns may have led to a rise in dengue cases, highlighting
71 the crucial role of vector control in disease prevention. Similar pathology of DENV and
72 COVID-19 presented diagnostic challenges, potentially contributing to underreporting (4) (6)
73 (7) (8) (9).

74 Some studies indicate that ADE due to prior SARS-CoV-2 infection may elevate the risk of
75 symptomatic and/or severe dengue. In Pakistan, a significant increase in dengue-related deaths

(linked to DENV-2 prevalence) was observed in patients with a pre-exposure to SARS-CoV-2 (10).

Modest serological cross-reactivity between SARS-CoV-2 and DENV-2 has been reported (11) (12) (13). However, it is unclear if this would have any clinical impact on dengue cases (14). A study reported rabbit IgG against purified SARS-CoV-2 S1-RBD cross-reacts with DENV Envelope (E), precursor-membrane (PrM), and Non-structural protein 1 (NS1). However, these antibodies did not enhance DENV infection in THP-1 cells expressing FcR. Moreover, they impeded DENV infection at high concentrations (15). Another study showed *in vitro* inhibition of dengue infection by sera from convalescent COVID-19 patients' sera (16).

Nath *et. al.* demonstrated serological cross-reactivity of SARS-CoV-2 positive serum samples with DENV1 and that the sera neutralized DENV1 (16). Anti-S1-RBD antibodies were shown to impede DENV infection at a specific concentration and COVID-19 patients' sera exhibited a neutralizing ability against dengue infection (15)**.** El-Qushayri *et al.,* in their systematic review, aimed to assess the clinical outcomes of patients with dengue and COVID-19 co-infection. They reported a high mortality rate in co-infected patients (19.1%), significantly exceeding the estimated global mortality rates for dengue (1.3%) and COVID-19 (2.04%). Also, they found that the hospital stay duration for co-infected individuals was longer than the reported median stays for standalone COVID-19 and dengue cases (17). Although, insightful, more information on the stoichiometry of the virus and antibodies in these studies, would have been useful, since it is crucial for understanding antibody-virus interactions and the potential for ADE

Here, we evaluated the effect of preexisting SARS-CoV-2 antibodies on DENV-2 infection using cell-based assays and mouse model of DENV infection.

Results:

100 ***In silico* interaction mining drives the cross-recognition of DENV-E protein by anti-**
101 **Spike and anti-RBD SARS-CoV-2 antibodies**
102 To assess the cross-reactivity of SARS-CoV-2 Spike antibodies with DENV-2 E-protein dimer
103 we used an *in silico* approach (Fig. 1A, B). We selected a panel of reported SARS-CoV-2
104 antibodies, based on their structure data (extent of their characterization, availability of the
105 structure information of their co-crystals with low resolution, preferably below 4 A°.) and
106 biological relevance (neutralization potential against SARS-CoV-2, target epitopes, etc.; Table-
107 S1). For the identification of DENV-2 E epitopes, C8 antibody against E-protein dimer (Fab
108 region, PDB-id: 4UTA) was used to characterize the interaction site based on interaction
109 fingerprinting. For identifying the cross-reactive antibodies forming the most promising
110 complexes with the E-protein; selected SARS-CoV-2 antibodies' protein-protein (PP) blind
111 docking was carried out with the whole DENV-2 E dimer. The consensus docked poses
112 obtained from Piper and HDOCK tools were used for post-docking qualitative and quantitative
113 analysis (pose selection and pose-filtering criteria). The top three SARS-CoV-2 antibodies
114 forming the complexes with DENV-2 in terms of docking energy, interaction fingerprinting
115 with co-crystal and MM-GBSA scores are CR3022 (Fab region, PDB-id:6W7Y), S2E12 ab
116 (Fab region, PDB-id:7K45) and DMAb 2196 (Fab region, PDB:8D8R) (Fig. 1C).
117 To quantitate their binding association at the residue level, major contributing amino acids were
118 identified by residue-wise decomposition analysis setting the cut-off value of -1·5 kcal/mol.
119 For the C8 antibody (4UTA) binding with DENV-2 E-protein, the interacting epitopes were
120 majorly localized in Domain II (Fig. 1D). The binding sites of CR3022, S2E12 ab, and DMAb
121 2196 antibodies were found to overlap with C8 binding site (Fig. 1D). The contributing residues
122 for all three antibodies were majorly located in Domain II including Fusion loop (Figure 1E,
123 F). The findings of overlapping residues between C8 and the three SARS-CoV-2 interacting
124 antibodies corroborate well with previously reported study (18). From the interaction analysis,

125 the R73 appeared as the most common interacting residue in all antibodies. The pair-wise
126 interaction analysis confirmed considerable overlapping residues between SARS-CoV-2 and
127 DENV-2 antibodies (Figure 1E and 1F). Key residues that overlap between DENV-2 and at
128 least two antibodies of SARS-CoV-2 are R73 (common among all), T70, S72 (Domain-II), R99
129 and N103 (Fusion loop) and E311 (Domain-III). We also performed the mining of paratope
130 residues of SARS-CoV-2 antibodies with equal and/or increased interaction energy as C8 and
131 identified overlapping residues between C8 and CR3022 (Figure S1).
132 Overall, the interaction maps and per-residue energetic decompositions showed that there were
133 several common residues involved in the interaction of DENV-2-E with C8 and CR3022,
134 S2E12 ab and DMAb 2196 antibodies indicating a high likelihood of cross-reactivity (Figure
135 1G and 1H, Table S2). The paratope residues involved in interaction of E-protein with CR3022
136 were also identified (Table-S3) and their interactions were assessed (Fig. S2).
137
138 **SARS-CoV-2 spike antibody CR3022 cross-reacts with DENV-2 and enhances DENV**
139 **infection *in vitro***
140 Based on the computational outcomes, one of the antibodies, CR3022, which showed the
141 highest affinity with DENV-2 E protein, was studied further. Based on the dengue virus
142 susceptibility and cells monolayer robustness, we selected C6/36 cell line for confocal studies.
143 Confocal microscopy images of CR3022 showed a statistically significant cross-reactivity with
144 an average Mean Fluorescence Intensity (MFI) of 7·68 (p-value<0·0001) (Fig. 2A). Bio-Layer
145 Interferometry (BLI), showed high affinity with a dissociation constant (KD) of <1·0pM with
146 Spike protein (Fig. 2B(i)), and 2·83 μM with DENV-2 E-protein (Fig. 2B(ii)). Further, we
147 observed a significant augmentation in the percentage of infected cells with CR3022 antibody
148 (p-value=0·01) in comparison to untreated virus control (Fig. 2C).
149

150 **SARS-CoV-2 convalescent plasma enhances DENV infection *in vitro***

151 Samples from convalescent COVID-19 patients (n=48, Table-S4) from different time intervals
152 of the pandemic were tested for their ability to cause ADE. We used FcγR-I, II and III
153 expressing K562 and U937 cell lines. Both cell lines were shown to predominantly express
154 FcγR-II (Fig. S3), as reported previously (19). The basal value of the only virus infection
155 obtained in cell lines are normalized to the tested samples in order to calculate the fold change
156 and graphs are plotted against virus infection (no serum) vs virus infection (incubated with
157 serum) in tested samples. The DENV-2 infected K562 cells were observed to increase from 1
158 to 236 times in the first set of convalescent samples (recovered individuals during Wuhan
159 wave), 77 to 235 times in the second set of convalescent samples (recovered individuals
160 during/around the delta wave), and 44 to 172 times in the third set of convalescent samples
161 (recovered individuals during omicron wave), compared to untreated virus control (Fig. 3A-D).
162 The FACS gating strategy is given in Fig. S4. Using a subset of the convalescent plasma
163 samples (n=15) similar results were observed in U937 cells, where DENV-2 infection was
164 enhanced in the range of 32 to 292 times as compared to the virus control (Fig. S5A-B). A virus
165 neutralization assay with SARS-CoV-2 Wuhan strain (Table-S5), did not show any association
166 between the neutralizing antibody titer and the ADE titers (Fig. S6A-C). Similarly, we did not
167 find any association of ADE titers with disease severity in patients with COVID-19 (Fig. S6D).
168 A representative quantitative PCR assay for intracellular DENV-2 genomic RNA showed a
169 higher viral load in 70% of COVID-19 convalescent plasma treated samples as compared to the
170 control (Fig. S7). This data correlates with the increase in DENV-2 positive cells observed in
171 flow cytometry. Determination of the infectious titer of DENV produced from infected cells by
172 focus-forming unit assay also showed a significant increase in the Foci-forming units/ml
173 (FFU/ml) in COVID-19 convalescent plasma treated samples as compared to control (Fig. S8).
174

175 **SARS-CoV-2 antibodies enhance dengue virus infection *in vivo***

176 To validate the *in silico* and *in vitro* findings, we performed *in vivo* experiments where we took
177 21 AG129 (Immunocompromised, lack of IFNAR1 and IFNGR1) mice within 6-8 weeks age
178 group. The mice were divided into three groups, Group 1 as mock (G1, N=5), Group 2 as
179 dengue virus control (G2, N=8), and Group 3 as test with both SARS-CoV-2 and dengue virus
180 infection (G3, N=8). G2 was infected with dengue virus infection at day 21 and G3 was infected
181 with SARS-CoV-2 virus at day 0 followed by dengue virus infection at day 21. Both G2 and
182 G3 mice were infected with adeno-ACE-2 (Ad5CMVh, The University of Iowa Viral Vector
183 Core Facility) viral vector at -5 days which is essential for SARS-CoV-2 infection. Body weight
184 was observed for all the animals till day 27 when they were euthanized as shown in the
185 schematic experimental plan (Fig. 4A). Average body weight in G2 mice group decreased at
186 day 3 but it recovered with time (Fig. 4B). A significant decrease of body weight was observed
187 in G3 as compared to G2.

188 We further tested the antibody response against SARS-CoV-2 spike antigen at day 21 before
189 DENV-2 infection, we observed the anti-spike IgG antibody response in all mice in G3 (Fig.
190 4C). Next, the live dengue virus particles determined in serum samples collected on day 27
191 (Fig. 4D), the data revealed a notable increase in number of viral particles in G3 mice group as
192 compared to G2 mice group indicating enhancement of dengue infection with SARS-CoV-2
193 virus. Next, we tested the viral replication in the liver and spleen of the infected mice. We
194 observed a high copy of viral RNA both in liver (Fig. 4E) and spleen (Fig. 4F) tissues. We also
195 observed a decrease in the platelet count, as previously reported to occur during dengue
196 infection. As shown in Fig. 4G, a decrease in the platelet count was seen in G1 vs G2 and G3
197 however, we did not observe any significant difference in G2 vs G3. WBC and Hematocrit
198 measurement was also carried out but no significant differences in G2 vs G3 groups (Fig. 4H
199 & 4I) were observed.

200

201 **SARS-CoV-2 spike antibodies cross-react with DENV**

202 We wanted to check if the available sera/ antibodies cross react with DENV-2. To do that,
203 SARS-CoV-2 anti-spike polyclonal antibody raised in rabbit (P1R) and mice (MSer) (obtained
204 from BEI resources USA) were analysed for cross-reactivity with DENV-2. Using confocal
205 microscopy, we observed that both showed a significant cross-reactivity with an average (MFI)
206 of 13·2 for P1R and 13·4 for MSer (Fig. 5A-B). Mouse Monoclonal antibodies against SARS-
207 CoV-2, 1A9 (MFI of 7.4) and MM41 (MFI of 1.57), also showed cross-reactivity with DENV-
208 2. The positive-control, 4G2 (pan-flavivirus-anti-envelope antibody), showed MFI of 18·28
209 whereas the Negative-control, anti-Rabies monoclonal (Rabishield®), showed no reactivity
210 with DENV-2. The binding kinetics of 1A9 (SARS-CoV-2 spike antibody) showed a high
211 affinity to DENV-2 Envelope with a dissociation constant (KD) of 4·84 μM (Fig. 5C ii-iii)
212 using Bio-Layer Interferometry (BLI).

213

214 **SARS-CoV-2 spike antibodies enhance DENV-2 infection**

215 Since DENV is endemic to India pre-existing anti-DENV antibodies may be responsible for the
216 observed ADE. To rule out this possibility, we further tested commercially available
217 monoclonal and polyclonal antibodies and sera raised in-house against the SARS-CoV-2 spike
218 and RBD for their potential to enhance the DENV-2 infection (Table-S6). All of the tested
219 antibodies (M1B, 1A9, MM41, P1R, M4B, M5B, Hser) enhanced DENV-2 infection (Fig. 6).
220 The RBD specific antibody (M5B) showed stronger enhancement compared to the antibody
221 against spike (MM41) with a dose-dependent increase in DENV-2 infection (Fig. 6A-B).
222 Similarly, hamster serum against purified SARS-CoV-2 spike protein also showed ADE of
223 DENV-2 infection in K562 cells (Fig. 6C). Monoclonal antibody against Rabies virus
224 (Negative-control), did not show any ADE of dengue infection in K562 cells (Fig. 6C). A

225 similar ADE of DENV infection was observed in U937 cells too (Fig. S9). Three monoclonal
226 antibodies – 4G2, 1A9, and M4B, showed significant ADE, as determined by the infectious
227 titer of the virus released in the culture supernatant from K562 cells (p-value<0·0001; Fig. S10).
228 Having established that there is an enhancement of DENV-2 infection due to anti-SARS-CoV-
229 2 antibodies, we next investigated whether it is time-dependent. We assessed ADE at 6 h, 18 h
230 and 36 h post-infection (Fig.S10). Mice (Mser) and hamster (Hser) sera, showed significant
231 ADE with respect to virus control (adjusted p-values Mser=0·0071 and Hser=0·0001), even at
232 6 hpi (Fig. S10). Although, we didn't observe a significant enhancement due to 4G2 and anti-
233 Spike monoclonals M3S and M2G at 6 hpi. At 18 hpi, a significant increase in the DENV-2
234 positive cells with respect to virus control was observed in 4G2 as well as M2G (Adjusted p-
235 value=0·0101), which further enhanced significantly at 36 hpi (Adjusted p-values 4G2=0·0001
236 and M2G=0·0035). The ADE in Hser reached saturation as early as 6 h (Adjusted p-
237 value<0·0001).
238
239 **Discussion:**
240 In this study, we demonstrate that SARS-CoV-2 antibodies cross-react with DENV-2 and
241 enhance DENV infection. A thorough *in silico* study indicated the high likeliness of cross-
242 reactivity of SARS-CoV-2 spike antibodies with DENV-2 E protein. SARS-CoV-2 spike
243 protein is critical for viral entry into cells and is the major target not only for neutralizing
244 antibodies but also for infection-enhancing antibodies (20). The *in silico* results indicated that
245 there is a significant interaction of SARS-CoV-2 antibodies with DENV-2 dimeric E protein.
246 The binding free energy of SARS-CoV-2 antibodies for example, CR3022 (6W7Y), S2E12 ab
247 (7K45) and DMAb2196 (8D8R), being comparable to the DENV-2 dimer specific antibody,
248 C8 (4UTA). These top three binders (SARS-CoV-2 specific antibodies) shared their interacting
249 interface with C8 antibody. The residues involved in the interaction of C8 antibody with

250 DENV-2 E, were also involved in the interaction of at-least one of the top three binders with
251 E-protein. The contributing residues which were found to be majorly stabilizing the interaction
252 of these top three SARS-CoV-2 antibodies with E-protein. We also observed that convalescent
253 plasma samples of SARS-CoV-2 recovered individuals, collected at three different time
254 intervals during COVID 19 pandemic, significantly enhanced the DENV-2 infection in cultured
255 Fc-receptor positive K562 and U937 cells. We observed an increased viral load as indicated by
256 FFU and also increased viral RNA levels in spleen and liver (Fig. 4d, e, f) in AG129 mice group
257 which had SARS-CoV-2 antibodies. The finding in animals model strongly supported our *in*
258 *silico* and *in vitro* data which clearly showed that SARS-CoV-2 spike antibodies mediated
259 enhancement of dengue virus infection.
260 Our work supports the work published by others highlighting SARS-CoV-2 cross-reactivity
261 with dengue virus and false positivity with dengue serology (21) (22). We used the DENV-2
262 envelope protein for BLI and computational studies since it has been reported to have maximum
263 cross-reactivity with SARS-CoV-2 S1 specific antibodies (11). The dimeric DENV-2 E-protein
264 was used for docking studies as we intended to study the interaction of DENV-2 with SARS-
265 CoV-2 spike antibodies, which would happen before the viral entry, extracellularly and it's
266 known that the E-protein exists as a head-to-tail oriented homodimer on the surface of mature-
267 virions (23). All the residues involved in the interaction of the top three binders of SARS-CoV-
268 2 antibodies with E-protein when mapped, were majorly found to lie in the Domain-II and
269 fusion-loop of E-protein. It is well known that the antibodies against two epitopes of DENV are
270 strong mediators of ADE: prM epitopes (24) and fusion loop epitopes (25). The fusion loop
271 epitopes could be the ones, potentially involved in ADE. Multiple residues have been identified
272 from *in silico* interaction mining, among them few residues such as R73 (common among all),
273 T70, S72 (Domain-II), R99 and N103 (Fusion loop) and E311 (Domain-III) seem critical. These
274 residues put forth the possible avenue to explore further for epitope-based therapeutic

275 interventions. The BLI findings between dengue envelope protein and antibodies against
276 SARS-CoV-2 spike protein indicate a strong interaction with KD values in μM range.
277 The DENV-2 used for the *in vitro* assay was prepared in C6/36 cells and wasn't characterized
278 for the proportions of immature and mature-virions. It is well known that the virus prepared *in*
279 *vitro* in mosquito cells has a considerably greater number of immature virions as compared to
280 mammalian cells, probably due to differential furin-expression (26) (27). Also, it is recognized
281 that laboratory adapted DENV strains are more dynamic than clinical strains and expose cryptic
282 epitopes more easily (28). Thus our virus preparation might have major proportion of immature
283 virions but this probably won't change the fact that the ADE of DENV-infection would happen
284 since the viral heterogeneity in response to the natural DENV-infections is also well known
285 The antibody repertoire in the natural infections is known to have an abundance of poorly
286 neutralizing antibodies which are majorly generated in response to the immature conformations
287 (29), which is a result of incomplete furin processing, resulting in egress of immature-forms
288 along with and mature-forms of virions post-assembly (30) (31). Also, the fully mature-virions
289 have been reported to be less susceptible to neutralization by cross-reactive and heterotypic
290 immune sera than partially mature variants (29)**.** Thus, the heterogeneity in the DENV-2
291 preparation used for the *in vitro* assays can be probably closely related to the natural infection
292 scenario. Although we did not have the history of patient's (SARS-CoV-2 Convalescent
293 samples) earlier infection from other dengue serotype which could have resulted in ADE in our
294 finding, we tested the commercially available SARS-CoV-2 antibodies and Spike-immunized
295 mice and hamster sera. Monoclonal and polyclonal antibodies raised against SARS-CoV-2
296 showed an increased DENV-2 infection in both cell-based models which re-confirms our
297 observations. Due to limitation on dengue virus serotypes, we only tested ADE against Dengue
298 serotype 2 but we believe that we will have similar ADE effect as all the dengue serotypes are
299 very closely antigenically related. However, in the animal experiment, the platelet, WBC counts

300 and hematocrit levels were not significantly affected between mice given dengue (G2) and
301 SARS CoV-2 + DENV (G3). As these parameters are associated with disease severity which
302 could explain why we did not observe dengue severity during the SARS-CoV-2 pandemic
303 which are promoting us to dig more deeper and further studies to find the missing links. We
304 also observed an increase in dengue viral load in G3 (SARS CoV-2 + DENV infected) group
305 mice as compared to G2 (dengue infected) group mice, that might be indicating an increase in
306 the number of the symptomatic cases in endemic population rather asymptomatic cases. It is
307 still not clear if there was underreporting or reduced testing for dengue during the peak SARS-
308 CoV-2 pandemic as the clinical symptoms of both viruses are very similar. Our understanding
309 is still limited and future studies might shed some light on the this.
310 The limitation of the study is the availability of the pre-pandemic clinical samples like
311 plasma/Serum or PBMCs, which could have provided a better insight and might have shed
312 some light on why these all are not leading to dengue severity in the real-world scenario. We
313 tried to overcome this using the animal model but a clinical sample would have been better
314 comparator.
315 Based on the current finding from *in silico, in vitro and in vivo* experiments, the study suggest
316 that SARS-CoV-2 spike directed antibodies cross reacts with dengue envelope protein and
317 enhance dengue viral load in AG129 experimental mice. Our findings signify the importance
318 of the cross reactivity and viral interactions in endemic regions where more than one virus is
319 circulating at the same time. Understanding the viral interactions during the co-circulation/Co-
320 infections needed more research in future to understand how they pose vaccine development
321 challenges and will impact on public health. These things will also pose significant challenges
322 on surveillance and/or vaccine running programs which might provide a false positivity due to
323 viral cross reactivity. So having an assay which can clearly differentiate the viral infection will
324 be more beneficial approach in future.

325

326 **Materials and Methods:**

327 **Molecular docking of DENV-2 Envelope glycoprotein and SARS- CoV-2 antibodies:**

328 **Curation of data:**

329 X-ray crystal structures of DENV-2 envelope glycoprotein (PDB ID:4UT6) (32) and SARS-
330 CoV-2 antibodies were curated from RCSB in PDB format (http://www.rcsb.org/pdb). These
331 crystal structures along with their corresponding resolution values, and are summarized in –
332 Table-S1. Crystal structure of antibodies were curated by removal of spike protein, water
333 molecules and metal ions using UCSF Chimera 1·15 (33). All structures were prepared using
334 Maestro's Protein Preparation Wizard module (Schrödinger Release 2020-1) (34). The
335 hydrogens and bond orders were added, missing side-chains and loops were filled by Prime
336 (34). The hydrogen bond (HB) optimization and restrained minimizations were also done for
337 the systems using force field OPLS4 (35).

338 **Protein-Antibody docking and choosing the best pose:**

339 Protein-protein interactions govern various aspects of structural and functional cellular
340 mechanisms, and their elucidation is crucial for a better understanding of biological processes.
341 All the prepared SARS-CoV-2 antibodies, along with controls i.e positive (pdb-id:4UTA) and
342 negative control (pdb-id:7U9G) were docked on prepared DENV2 E protein structure by
343 masking non-CDR regions of antibodies. The Chothia definition is used for the CDR region.
344 Multiple docking methods were used to minimize the biases by including HDOCK (36),
345 pyDock (37) and Piper program (38). The rationale for implementing multiple docking
346 programs was to obtain the consensus results from all three tools and to remove any false-

347 positive outcomes. Best poses were chosen from docked models on the basis of their docking
348 score, cluster size (39) and reported paratope residues (40) (41) (42).

349 **Thermodynamic quantification using Molecular Mechanics-Generalized Born Surface**
350 **Area (MM-GBSA):**

351 The binding free energy of protein and antibody complexes was carried out in Prime MM-
352 GBSA (Molecular Mechanics Generalized Born Surface Area) by Prime (43) module of
353 Schrodinger suite. We used the VSGB solvation model and OPLS4 force field. The binding
354 free energy is calculated by: MMGBSA dG Bind (NS) = Complex – Receptor (from optimized
355 complex) – Ligand (from optimized complex) = MMGBSA dG Bind–Rec Strain–Lig Strain,
356 Where, Rec Strain = Receptor (from optimized complex) – Receptor, Lig Strain = Ligand (from
357 optimized complex) – Ligand, MMGBSA dG Bind = Complex – Receptor – Ligand, NS = no
358 strain.

359 **Figures:**

360 All figures were generated using VMD (V.1·9·1) (44) and graphs were generated using the
361 XMGRACE (Version 5·1·19) (42).

362 **Cells:**

363 Human myeloid cell lines K562 (ATCC CCL-243) and U937 (ATCC CRL-1593.2) were
364 cultured in Iscove's Modified Dulbecco's media (IMDM, HIMEDIA) and Roswell Park
365 Memorial Institute (RPMI, Gibco) 1640 respectively. African Green Monkey cell line Vero E6
366 (NCCS, India) was maintained in Dulbecco's Modified Eagle Medium (DMEM, HIMEDIA)
367 while A. albopictus cell line C6/36 (NCCS, India) was cultivated in Leibovitz's L-15 Medium
368 (HIMEDIA). All the cells were maintained in respective media supplemented with 100 U/ml

369 of penicillin, 100 µg/ml of streptomycin (HIMEDIA), and 10% Fetal Bovine Serum
370 (HIMEDIA). C6/36 cells were maintained at 28°C (ESCO incubator) without CO_2 while the
371 other cells were grown in a humidified 37°C incubator (Thermo Fisher Scientific) with 5%
372 CO_2.

373 **Virus stocks:**

374 Dengue virus serotype 2 (NGC strain) was propagated in C6/36 cells and it was used for all the
375 assays. The cells at a confluency of 60-70% were infected with Dengue virus at a multiplicity
376 of infection (MOI) of 0·1 using inoculum prepared in L-15 medium supplemented with 2%
377 FBS. It was incubated with cells for 2 h at 28°C with intermittent rocking. Subsequently, the
378 cells were washed and incubated with L-15 medium with 10% FBS. Culture supernatant was
379 harvested at 5 dpi, clarified by centrifugation at 129 ×*g* at room temperature and concentrated
380 using centrifugal ultrafiltration (Amicon® Ultra centrifugal filter (100 kDa), ACS510024 from
381 Millipore, Darmstadt, Germany) at 3220 ×*g* for 10 min for every 15 ml of supernatant. The
382 infectious titer of the virus was determined by a focus-forming unit (FFU) assay performed in
383 Vero E6 cells.

384 The three variants of SARS-CoV-2, original Wuhan (USA-WA1/2020, Genbank: MN985325),
385 B·1·617·2 (δ-variant) known as THSTI_287 (GenBank: MZ356566·1), and Omicron
386 BA·1(GISAID accession no.: EPI_ISL_8764350) were propagated in Vero E6 cells. Cells were
387 infected with 0·1 MOI of virus inoculum and incubated for 1 h with shaking at 37°C. Virus
388 supernatant was harvested at 48 hpi, filtered, and stored at -80°C. The infective titer was
389 determined by titration on Vero E6 cells using the $TCID_{50}$ method (45). These virus stocks were
390 used for neutralization assays.

391 **Serum samples and Antibodies:**

392 We selected a group of convalescent plasma samples (n=48) collected at three different time
393 intervals during COVID-19 pandemic in India. They are defined as follows: the first interval
394 was from May 2020 to January 2021, second interval from May 2021 to June 2021, third
395 interval from February 2022 to April 2022. The clinical details of the samples are given in the
396 Table S1. The pan flavivirus, anti-envelope mAb, 4G2 was purified inhouse from HB112
397 hybridoma cells. SARS-CoV-2 spike (S2 specific) antibody 1A9 was purchased from Gentex
398 while Anti- Recombinant SARS-CoV-2 Spike Protein (whole spike) Sino 4059-MM41 was
399 purchased from Sino Biologicals. Other SARS CoV2-related antibodies M1B, M4B, M5B, P1R
400 were obtained from BEI resources, USA. SARS CoV2 infected mice and hamster serum were
401 generated inhouse. Rabies Human monoclonal antibody, Rabishield®-100 (Serum Institute of
402 India), was purchased from the pharmacy. All the details regarding commercial antibodies/
403 serum are mentioned in - Table S2.

404 **Confocal microscopy:**

405 0.5 x 10^6 C6/36 cells from an exponentially growing culture were seeded on grass cover slips
406 followed by DENV-2 at 1.0 MOI. At 48 h post-infection the cells were fixed with 3.7%
407 paraformaldehyde (PFA) and permeabilized using 0.1% Triton-X-100. The cells were immune-
408 stained with primary antibody and fluor-conjugated secondary antibodies. Subsequently,
409 coverslips were mounted onto glass slides using ProLong Gold Antifade Mountant
410 supplemented with DAPI. Fluorescence was observed under 60X magnification using a
411 FLUOVIEW FV3000 confocal microscope (Olympus). The mean fluorescence intensity (MFI)
412 was calculated using images from 10 fields per slide with 7 cells per field (at least 70 data
413 points). Statistical analysis employed One-way ANOVA followed by Dunnett's test, comparing
414 to the negative control (Rabishield).

415 **Live Virus Neutralization Assay:**

416 Two-fold serial dilutions of heat-inactivated plasma samples were mixed with 100 $TCID_{50}$ of
417 SARS-CoV-2 virus and subsequently allowed to infect Vero E6 monolayers. After incubation
418 for 72 h at 37°C with 5% CO_2, the degree of CPE was qualitatively determined under a
419 microscope. Absence of CPE indicated virus neutralization, and the highest dilution that
420 completely prevented emergence of CPE was considered as the neutralization titer. For plasma
421 samples collected during-the third interval, cells were fixed 24 h post-infection and immune-
422 stained using antibody against the SARS-CoV-2 Nucleocapsid protein (1:2000, 4H2,
423 Genscript), followed by Alexa 488 conjugated anti-mouse antibody (1:500, Invitrogen).
424 Fluorescent foci were quantified by AID iSpot Reader with AID EliSpot 8.0 iSpot software.

425 **Antibody-dependent Enhancement (ADE) Assay:**

426 Serum samples (15 µl) and commercial antibodies (5 µl) were diluted in plain Iscove's Modified
427 Dulbecco's Medium (IMDM) to a total volume of 100 µl. Subsequently, 100 µl of virus dilution
428 was added, and the mixture was incubated at 37°C for 1 h. The virus-antibody complexes were
429 then allowed to infect 1 x 10^6 cells K562/U937 cells for 2 h at an MOI 1. After infection the
430 cells were washed and incubated in IMDM-2% FBS at 37°C, 5% CO_2 for 36 h. Subsequently,
431 cells were fixed using 4% PFA, permeabilized with 0.1% Triton X-100, immune-stained with
432 purified 4G2 (dilution 1:200), and Alexa-Fluor 488 conjugated anti-mouse (dilution 1:500).
433 The number of cells positive for DENV antigen was quantified by flow cytometry.

434 **Flow Cytometry Analysis:**

435 Flow cytometry was conducted using a BD FACS Canto II flow cytometer (BD Biosciences)
436 with 20,000 cells acquired per sample through FACS Diva software. FlowJo v10.8.1 was used
437 for analysis. Live cells were gated based on FSC and SSC, followed by singlet determination
438 using FSC-A vs FSC-H gate. Dengue virus-positive cells were gated on the FITC channel using

439 singlet population. FITC voltage was set using isotype control. Fcγ receptor expression was
440 assessed with anti-CD64 (Alexa Fluor 700), anti-CD32 (PE), and anti-CD16 (APC) antibodies
441 in K562 and U937 cells. Statistical analysis was conducted in GraphPad Prism 8.

442 **Detection of DENV RNA using Quantitative RT-PCR:**

443 Total RNA from 1 x 10^6 K562 cells was extracted using the standard TRIzol method. RNA was
444 quantitated using Nanodrop (Thermofisher Scientific) and 300 ng RNA was used for qPCR
445 using a one-step RT-PCR kit (SOLIScript® 1-step Probe kit, Solis Biodyne) following the
446 manufacturer's protocol for detection of DENV2 RNA. GAPDH was used as an internal
447 control. Fold change in DENV2 RNA copies was calculated with respect to GAPDH. The
448 details regarding primer and probe sequences are given in Table S7.

449 **Binding kinetics using Biolayer Interferometry (BLI):**

450 BLI studies were performed on an Octet RED 96 instrument at 24°C with shaking at 1000 rpm
451 (ForteBIO). For DENV-2 Envelope protein, the buffer composition was 50mM Tris, 150mM
452 NaCl, 0.5% glycerol, pH 8.0. Whereas, for SARS-CoV-2 Spike protein, phosphate buffered
453 saline, pH 7.4 was used. Sensors were in the respective kinetic buffer (46). For studying binding
454 kinetics with protein E, antibodies at a concentration of 5 µg/ml were loaded onto the sensors
455 (AHC (Anti-hIgG Fc Capture) for CR3022 and C8, protein G (for 1A9 antibody)) DENV E
456 dimeric protein was diluted serially three-fold (starting with 6000nM) and Spike trimeric
457 protein was diluted 2-fold (starting with 600nM) in their respective kinetic buffers. The
458 designed experiment started with a baseline (100Sec), followed by 3 cycles of neutralization
459 and regeneration and again a baseline (100Sec). After this step, antibody loading was performed
460 (700sec) onto all the 5 sensors. After the loading step, another baseline (baseline2, 60sec),

461 Association was performed after the 2nd baseline step for 300sec, followed by 300sec
462 dissociation.

463 Here the 5th sensor was used as reference where no analyte was used, where the analyte
464 concentration was kept 0nM. The same sensor during the data processing was assigned as
465 reference well (change well type-reference well) and same wells; reference well, were
466 subtracted from the raw data. Here the ligand and analyte dilution as well as the whole
467 experiment was performed in the respective kinetic buffers. The binding responses were
468 calculated and fitting globally with a 1:1 binding model using ForteBio's Data Analysis
469 software 10·1. The data was considered validated if $X^2 < 0{\cdot}5$.

470 **Mouse Infection**

471 The AG129 (IFNα/β/γR -/- 129/Sv) mice were obtained from the Jackson laboratory, USA
472 and maintained in small animal facility (SAF), RCB, Faridabad, India. All experiments with
473 AG129 mice were performed in 6-8 weeks old mice of either sex. One group of mice were
474 treated (one-time through intranasal route) with human ACE2 adenovirus using 2.5×10^8 PFU
475 for transient expression of hACE2 in lungs and respiratory track. After five days mice were
476 infected with SARS-CoV-2 via nasal route inoculation using 1×10^5 PFU virus. Mice were
477 bled at day7, 14 and 21 post SARS-CoV-2 infection to measure the antibodies against SARS-
478 CoV-2. At day 21 both the groups were challenged with 1×10^4 FFU mouse-adapted DENV2
479 (P8-P23085 INDI-60) and were euthanized on the moribund state.

480 **Focus forming unit (FFU) assay**

481 FFU assay was carried out to determine the virus titer in the serum of DENV2 infected
482 AG129 mice with slight modifications. Vero E6 cells were seeded at a density of 0.01×10^6
483 cells/well in a 96-well black/clear bottom plate and cells were allowed to reach 80%

484 confluency. At 80% confluency 100 µl of 10-fold serially diluted serum in media with 2%
485 FBS was added to the wells and incubated. After 2 hr, serum was removed, fresh media with
486 2% FBS was added and incubated for 24 hr at 37° C in 5% CO_2. Following that cells were
487 fixed with 2% PFA and the immunostaining for virus detection was performed using mAb
488 4G2 (pan-DENV anti-envelope antibody), followed by secondary antibody, goat anti-mouse
489 IgG, AF488 conjugated (Invitrogen) prepared in permeabilization buffer (0.1% triton x100
490 with 2%BSA in PBS). The foci were visualized and counted using fluorescence microscope.

491 **Quantitative real time PCR**

492 Total RNA from the mice tissues was extracted using RNAiso (Takara Bio, Japan) followed by
493 phenol-chloroform treatment. The first strand cDNA was synthesized from 1µg RNA using
494 cDNA synthesis kit (BioRad, USA) as per manufacturer's protocol. The cDNA was used for
495 real-time PCR using SYBR green supermix (BioRad) in an Applied Biosystems Quant
496 Studio™ 6 Flex Real-Time PCR System. The primers set used for detection of the respective
497 genes are given in Table S8.

498 **Statistical analysis:**

499 Experimental values were represented as mean ± standard deviation (SD). Statistical analysis
500 was done using the ordinary one-way ANOVA followed by Dunnett's multiple comparison
501 test, using GraphPad Prism version 8·4·2. Differences were considered significant at p-value <
502 0·05.

503

504 **Acknowledgements:**

505 The following reagent was obtained through BEI Resources, NIAID, NIH: SARS-Related
506 Coronavirus 2, Isolate USA-WA1/2020, NR-52281, Monoclonal Anti-SARS-Related

Coronavirus 2 Spike Glycoprotein, Clone 1-3D7 (produced *in vitro*), NR-56488, Monoclonal Anti-SARS-Related Coronavirus 2 Spike Glycoprotein Receptor Binding Domain-(RBD), Clone 2TP1C3 (produced *in vitro*), NR-55296, Polyclonal Anti-SARS-Related Coronavirus 2 Spike Glycoprotein (IgG, Rabbit), NR-52947." The RBD is proprietary reagents with IP No. 202011018845, we thank Dr. Barney Graham (VRC/NIAID/NIH) for providing us with spike construct (SARS-2-CoV S 2P). We would like to thank Prof. Shinjini Bhatnagar, Prof. Pramod Garg and Prof. Jayanta Bhattacharya from THSTI for critically reviewing the manuscript, ABSL3 facility committee and staff for their help and support. This research has been conducted with the significant contribution and expertise of THSTI, NCR Biotech Science Cluster BIOREPOSITORY and DBT India Consortium".

DBT India Consortium**, ** Name of all the collaborating Institutes/ Hospitals: Translational Health Science Technology Institute, Clinical partners: Maulana Azad Medical College, Lok Nayak Jai Prakash Hospital, and Lady Hardinge Medical College in Delhi, ESI Medical College Hospital, Faridabad, Civil Hospital, Gurugram, Haryana; Civil Hospital, Palwal, Haryana; Al-Falah School of Medical Science & Research Centre and Hospital, Dhauj, Haryana; Medanta Hospital, Gurugram; Shaheed Hasan Khan Mewati Government Medical College, Nalhar, Haryana.

Data availability:

All the data are presented in this manuscript. The virus strains used in this study have the following accession numbers: original Wuhan (USA-WA1/2020, Genbank: MN985325), B·1·617·2 (δ-variant) known as THSTI_287 (GenBank: MZ356566·1), and Omicron BA·1 (GISAID accession no.: EPI_ISL_8764350) Source data are provided with this paper.

532 **Author Contributions:**

533 SM conceptualized the idea. SM, SB, SA, TrS and PG coordinated the research activity. KJ
534 and SS contributed to designing and execution of viral assays. KJ, SS, GS, NB, TS, MT, JK,
535 DKR, BL, SK, PS, SK, VP, S, LK and VG contributed to data curation, investigation and
536 methodology. KJ, SS, TRA, GJ, GS, SB, SA, TrS, PG and SM contributed to formal analysis.
537 SS, SR, MG, PK, NW, RT, SB, TrS, SA and SM provided resources. KJ, SS, TRA, GJ, TrS,
538 PK, NW, RT, SB, SA, PG and SM contributed to writing, review & editing the draft. All authors
539 had full access to all the data in the study and had final responsibility for the decision to submit
540 for publication.

541

542 **Ethics statement**

543 We obtained the approval from the Institutional Bio-Safety Committee and Review
544 Committee on Genetic Manipulation (RCGM), for *in vitro* and *in vivo* work, prior to
545 conducting the studies: (IBSC#495/2023), RCGM (No.-BT/IBKP/137/2020), RCGM
546 (No.BT/IBKP/053/ 2020).

547

548 **Disclosure statement**

549 The Author declares no conflict of interest.

550

551 **Funding:**

552 The current research is funded by the Translational Research Program Grant,
553 BT/PR30159/MED/15/188/2018, THSTI Core (Intramural P417) and the Bill and Melinda
554 Gates Foundation GIISER-South Asia (INV-030592). The computational work was supported
555 by the national network project (NNP-BT/PR40189/BTIS/137/50/2022), DBT. The work on
556 dengue envelope proteins was done with support of funding received from NBM (National

Biopharma Mission) scheme of BIRAC (Biotechnology Industry Research Assistance Council), India (BT/NBM099/02/18) (2019-2023). SK acknowledge NBM BIRAC for his fellowship support.

562 **Reference:**

563

564 1. WHO. WHO, Fact sheets / Detail / Dengue and severe dengue 2023 [cited 2023 11th
565 December]. Available from: https://www.who.int/news-room/fact-sheets/detail/dengue-
566 and-severe-dengue.
567 2. Lee MF, Voon GZ, Lim HX, Chua ML, Poh CL. Innate and adaptive immune evasion by
568 dengue virus. Front Cell Infect Microbiol. 2022;12:1004608. Epub 2022/10/04. doi:
569 10.3389/fcimb.2022.1004608. PubMed PMID: 36189361; PubMed Central PMCID:
570 PMCPMC9523788.
571 3. Pierson TC, Diamond MS. A game of numbers: the stoichiometry of antibody-
572 mediated neutralization of flavivirus infection. Prog Mol Biol Transl Sci. 2015;129:141-66.
573 Epub 2015/01/18. doi: 10.1016/bs.pmbts.2014.10.005. PubMed PMID: 25595803; PubMed
574 Central PMCID: PMCPMC4910618.
575 4. Khan S, Akbar SMF, Yahiro T, Mahtab MA, Kimitsuki K, Hashimoto T, et al. Dengue
576 Infections during COVID-19 Period: Reflection of Reality or Elusive Data Due to Effect of
577 Pandemic. Int J Environ Res Public Health. 2022;19(17). Epub 2022/09/10. doi:
578 10.3390/ijerph191710768. PubMed PMID: 36078486; PubMed Central PMCID:
579 PMCPMC9518125.
580 5. Khan S, Akbar SMF, Nishizono A. Co-existence of a pandemic (SARS-CoV-2) and an
581 epidemic (Dengue virus) at some focal points in Southeast Asia: Pathogenic importance,
582 preparedness, and strategy of tackling. Lancet Reg Health Southeast Asia. 2022;4:100046.
583 Epub 2022/07/26. doi: 10.1016/j.lansea.2022.100046. PubMed PMID: 35873345; PubMed
584 Central PMCID: PMCPMC9296506 interest.
585 6. Lu X, Bambrick H, Pongsumpun P, Dhewantara PW, Toan DTT, Hu W. Dengue
586 outbreaks in the COVID-19 era: Alarm raised for Asia. PLoS Negl Trop Dis.
587 2021;15(10):e0009778. Epub 2021/10/09. doi: 10.1371/journal.pntd.0009778. PubMed
588 PMID: 34624031; PubMed Central PMCID: PMCPMC8500420.
589 7. Manna S, Satapathy P, Bora I, Padhi BK. Dengue outbreaks in South Asia amid Covid-
590 19: Epidemiology, transmission, and mitigation strategies. Front Public Health.
591 2022;10:1060043. Epub 2023/01/03. doi: 10.3389/fpubh.2022.1060043. PubMed PMID:
592 36589966; PubMed Central PMCID: PMCPMC9797821.
593 8. Oladipo HJ, Rabiu I, Tajudeen YA. Dengue virus and SARS-CoV-2 Co-infection
594 dynamics: An emerging threat among African countries. Ann Med Surg (Lond).
595 2022;82:104398. Epub 2022/08/30. doi: 10.1016/j.amsu.2022.104398. PubMed PMID:
596 36035770; PubMed Central PMCID: PMCPMC9394095.
597 9. Prapty C, Rahmat R, Araf Y, Shounak SK, Noor AA, Rahaman TI, et al. SARS-CoV-2 and
598 dengue virus co-infection: Epidemiology, pathogenesis, diagnosis, treatment, and
599 management. Rev Med Virol. 2023;33(1):e2340. Epub 2022/03/04. doi: 10.1002/rmv.2340.
600 PubMed PMID: 35238422; PubMed Central PMCID: PMCPMC9111128.
601 10. Rana MS, Usman M, Alam MM, Ikram A, Salman M, Umair M. Impact of previous
602 SARS-CoV-2 infection on the rate of mortality in dengue. A preliminary report from Pakistan.
603 J Infect. 2022;84(5):722-46. Epub 2022/01/27. doi: 10.1016/j.jinf.2022.01.027. PubMed
604 PMID: 35081438; PubMed Central PMCID: PMCPMC8783977 of interest.
605 11. Masyeni S, Santoso MS, Widyaningsih PD, Asmara DW, Nainu F, Harapan H, et al.
606 Serological cross-reaction and coinfection of dengue and COVID-19 in Asia: Experience from
607 Indonesia. Int J Infect Dis. 2021;102:152-4. Epub 2020/10/30. doi:

608 10.1016/j.ijid.2020.10.043. PubMed PMID: 33115680; PubMed Central PMCID:
609 PMCPMC7585717.
610 12. Alla D, Alla SSM, Vempati R, Bhatt H, Sultana Q, Bhatt S, et al. Dengue & COVID-19: A
611 Comparison and the Challenges at Hand. Cureus. 2022;14(11):e31877. Epub 2022/12/30.
612 doi: 10.7759/cureus.31877. PubMed PMID: 36579259; PubMed Central PMCID:
613 PMCPMC9792364.
614 13. Digwo DC, Elebe CP, Chigor VN, Madueke SN, Ezeh CK, Ike AC. Occurrence of False-
615 Positive Tests and Cross-reactions Between COVID-19 and Dengue With Implications During
616 Diagnosis: A Mixed Evidence Synthesis. Infectious Microbes & Diseases. 2023;5(2):64-75. doi:
617 10.1097/im9.0000000000000116. PubMed PMID: 02123149-202306000-00004.
618 14. Ulrich H, Pillat MM, Tarnok A. Dengue Fever, COVID-19 (SARS-CoV-2), and Antibody-
619 Dependent Enhancement (ADE): A Perspective. Cytometry A. 2020;97(7):662-7. Epub
620 2020/06/09. doi: 10.1002/cyto.a.24047. PubMed PMID: 32506725; PubMed Central PMCID:
621 PMCPMC7300451.
622 15. Cheng YL, Chao CH, Lai YC, Hsieh KH, Wang JR, Wan SW, et al. Antibodies against the
623 SARS-CoV-2 S1-RBD cross-react with dengue virus and hinder dengue pathogenesis. Front
624 Immunol. 2022;13:941923. Epub 2022/09/02. doi: 10.3389/fimmu.2022.941923. PubMed
625 PMID: 36045680; PubMed Central PMCID: PMCPMC9420930.
626 16. Nath H, Mallick A, Roy S, Kayal T, Ranjan S, Sengupta S, et al. COVID-19 serum can be
627 cross-reactive and neutralizing against the dengue virus, as observed by the dengue virus
628 neutralization test. Int J Infect Dis. 2022;122:576-84. Epub 2022/07/11. doi:
629 10.1016/j.ijid.2022.07.013. PubMed PMID: 35811081; PubMed Central PMCID:
630 PMCPMC9262656.
631 17. El-Qushayri AE, Kamel AMA, Reda A, Ghozy S. Does dengue and COVID-19 co-
632 infection have worse outcomes? A systematic review of current evidence. Rev Med Virol.
633 2022;32(5):e2339. Epub 2022/02/26. doi: 10.1002/rmv.2339. PubMed PMID: 35213764;
634 PubMed Central PMCID: PMCPMC9111070.
635 18. Srivastava M, Suri C, Singh M, Mathur R, Asthana S. Molecular dynamics simulation
636 reveals the possible druggable hot-spots of USP7. Oncotarget. 2018;9(76):34289-305. Epub
637 2018/10/23. doi: 10.18632/oncotarget.26136. PubMed PMID: 30344943; PubMed Central
638 PMCID: PMCPMC6188144.
639 19. Littaua R, Kurane I, Ennis FA. Human IgG Fc receptor II mediates antibody-dependent
640 enhancement of dengue virus infection. J Immunol. 1990;144(8):3183-6. Epub 1990/04/15.
641 PubMed PMID: 2139079.
642 20. Wahala WM, Silva AM. The human antibody response to dengue virus infection.
643 Viruses. 2011;3(12):2374-95. Epub 2012/02/23. doi: 10.3390/v3122374. PubMed PMID:
644 22355444; PubMed Central PMCID: PMCPMC3280510.
645 21. Yan G, Lee CK, Lam LTM, Yan B, Chua YX, Lim AYN, et al. Covert COVID-19 and false-
646 positive dengue serology in Singapore. Lancet Infect Dis. 2020;20(5):536. Epub 2020/03/08.
647 doi: 10.1016/S1473-3099(20)30158-4. PubMed PMID: 32145189; PubMed Central PMCID:
648 PMCPMC7128937.
649 22. Lustig Y, Keler S, Kolodny R, Ben-Tal N, Atias-Varon D, Shlush E, et al. Potential
650 Antigenic Cross-reactivity Between Severe Acute Respiratory Syndrome Coronavirus 2 (SARS-
651 CoV-2) and Dengue Viruses. Clin Infect Dis. 2021;73(7):e2444-e9. Epub 2020/08/17. doi:
652 10.1093/cid/ciaa1207. PubMed PMID: 32797228; PubMed Central PMCID:
653 PMCPMC7454334.

654 23. Modis Y, Ogata S, Clements D, Harrison SC. A ligand-binding pocket in the dengue
655 virus envelope glycoprotein. Proc Natl Acad Sci U S A. 2003;100(12):6986-91. Epub
656 2003/05/22. doi: 10.1073/pnas.0832193100. PubMed PMID: 12759475; PubMed Central
657 PMCID: PMCPMC165817.
658 24. Rodenhuis-Zybert IA, van der Schaar HM, da Silva Voorham JM, van der Ende-
659 Metselaar H, Lei HY, Wilschut J, et al. Immature dengue virus: a veiled pathogen? PLoS
660 Pathog. 2010;6(1):e1000718. Epub 2010/01/12. doi: 10.1371/journal.ppat.1000718.
661 PubMed PMID: 20062797; PubMed Central PMCID: PMCPMC2798752.
662 25. de Alwis R, Williams KL, Schmid MA, Lai CY, Patel B, Smith SA, et al. Dengue viruses
663 are enhanced by distinct populations of serotype cross-reactive antibodies in human
664 immune sera. PLoS Pathog. 2014;10(10):e1004386. Epub 2014/10/03. doi:
665 10.1371/journal.ppat.1004386. PubMed PMID: 25275316; PubMed Central PMCID:
666 PMCPMC4183589.
667 26. Murray JM, Aaskov JG, Wright PJ. Processing of the dengue virus type 2 proteins prM
668 and C-prM. J Gen Virol. 1993;74 (Pt 2):175-82. Epub 1993/02/01. doi: 10.1099/0022-1317-
669 74-2-175. PubMed PMID: 8429301.
670 27. Davis CW, Nguyen HY, Hanna SL, Sanchez MD, Doms RW, Pierson TC. West Nile virus
671 discriminates between DC-SIGN and DC-SIGNR for cellular attachment and infection. J Virol.
672 2006;80(3):1290-301. Epub 2006/01/18. doi: 10.1128/JVI.80.3.1290-1301.2006. PubMed
673 PMID: 16415006; PubMed Central PMCID: PMCPMC1346927.
674 28. Chaichana P, Okabayashi T, Puiprom O, Sasayama M, Sasaki T, Yamashita A, et al. Low
675 levels of antibody-dependent enhancement in vitro using viruses and plasma from dengue
676 patients. PLoS One. 2014;9(3):e92173. Epub 2014/03/20. doi:
677 10.1371/journal.pone.0092173. PubMed PMID: 24642752; PubMed Central PMCID:
678 PMCPMC3958444.
679 29. Beltramello M, Williams KL, Simmons CP, Macagno A, Simonelli L, Quyen NT, et al.
680 The human immune response to Dengue virus is dominated by highly cross-reactive
681 antibodies endowed with neutralizing and enhancing activity. Cell Host Microbe.
682 2010;8(3):271-83. Epub 2010/09/14. doi: 10.1016/j.chom.2010.08.007. PubMed PMID:
683 20833378; PubMed Central PMCID: PMCPMC3884547.
684 30. Pierson TC, Diamond MS. Degrees of maturity: the complex structure and biology of
685 flaviviruses. Curr Opin Virol. 2012;2(2):168-75. Epub 2012/03/27. doi:
686 10.1016/j.coviro.2012.02.011. PubMed PMID: 22445964; PubMed Central PMCID:
687 PMCPMC3715965.
688 31. Cherrier MV, Kaufmann B, Nybakken GE, Lok SM, Warren JT, Chen BR, et al.
689 Structural basis for the preferential recognition of immature flaviviruses by a fusion-loop
690 antibody. EMBO J. 2009;28(20):3269-76. Epub 2009/08/29. doi: 10.1038/emboj.2009.245.
691 PubMed PMID: 19713934; PubMed Central PMCID: PMCPMC2771083.
692 32. Rouvinski A, Guardado-Calvo P, Barba-Spaeth G, Duquerroy S, Vaney MC, Kikuti CM,
693 et al. Recognition determinants of broadly neutralizing human antibodies against dengue
694 viruses. Nature. 2015;520(7545):109-13. Epub 2015/01/13. doi: 10.1038/nature14130.
695 PubMed PMID: 25581790.
696 33. Pettersen EF, Goddard TD, Huang CC, Couch GS, Greenblatt DM, Meng EC, et al. UCSF
697 Chimera--a visualization system for exploratory research and analysis. J Comput Chem.
698 2004;25(13):1605-12. Epub 2004/07/21. doi: 10.1002/jcc.20084. PubMed PMID: 15264254.
699 34. Sastry GM, Adzhigirey M, Day T, Annabhimoju R, Sherman W. Protein and ligand
700 preparation: parameters, protocols, and influence on virtual screening enrichments. J

701 Comput Aided Mol Des. 2013;27(3):221-34. Epub 2013/04/13. doi: 10.1007/s10822-013-
702 9644-8. PubMed PMID: 23579614.
703 35. Lu C, Wu C, Ghoreishi D, Chen W, Wang L, Damm W, et al. OPLS4: Improving Force
704 Field Accuracy on Challenging Regimes of Chemical Space. J Chem Theory Comput.
705 2021;17(7):4291-300. Epub 2021/06/08. doi: 10.1021/acs.jctc.1c00302. PubMed PMID:
706 34096718.
707 36. Yan Y, Tao H, He J, Huang SY. The HDOCK server for integrated protein-protein
708 docking. Nat Protoc. 2020;15(5):1829-52. Epub 2020/04/10. doi: 10.1038/s41596-020-0312-
709 x. PubMed PMID: 32269383.
710 37. Pallara C, Jimenez-Garcia B, Romero M, Moal IH, Fernandez-Recio J. pyDock scoring
711 for the new modeling challenges in docking: Protein-peptide, homo-multimers, and domain-
712 domain interactions. Proteins. 2017;85(3):487-96. Epub 2016/10/26. doi:
713 10.1002/prot.25184. PubMed PMID: 27701776.
714 38. Kozakov D, Brenke R, Comeau SR, Vajda S. PIPER: an FFT-based protein docking
715 program with pairwise potentials. Proteins. 2006;65(2):392-406. Epub 2006/08/26. doi:
716 10.1002/prot.21117. PubMed PMID: 16933295.
717 39. Lorenzen S, Zhang Y. Identification of near-native structures by clustering protein
718 docking conformations. Proteins. 2007;68(1):187-94. Epub 2007/04/03. doi:
719 10.1002/prot.21442. PubMed PMID: 17397057.
720 40. Zhang L, Cao L, Gao XS, Zheng BY, Deng YQ, Li JX, et al. A proof of concept for
721 neutralizing antibody-guided vaccine design against SARS-CoV-2. Natl Sci Rev.
722 2021;8(8):nwab053. Epub 2021/10/23. doi: 10.1093/nsr/nwab053. PubMed PMID:
723 34676098; PubMed Central PMCID: PMCPMC8083607.
724 41. Shan S, Mok CK, Zhang S, Lan J, Li J, Yang Z, et al. A Potent and Protective Human
725 Neutralizing Antibody Against SARS-CoV-2 Variants. Front Immunol. 2021;12:766821. Epub
726 2021/12/31. doi: 10.3389/fimmu.2021.766821. PubMed PMID: 34966387; PubMed Central
727 PMCID: PMCPMC8710476.
728 42. Callaway HM, Zyla D, Larrous F, de Melo GD, Hastie KM, Avalos RD, et al. Structure of
729 the rabies virus glycoprotein trimer bound to a prefusion-specific neutralizing antibody. Sci
730 Adv. 2022;8(24):eabp9151. Epub 2022/06/18. doi: 10.1126/sciadv.abp9151. PubMed PMID:
731 35714192; PubMed Central PMCID: PMCPMC9205594.
732 43. Wang E, Sun H, Wang J, Wang Z, Liu H, Zhang JZH, et al. End-Point Binding Free
733 Energy Calculation with MM/PBSA and MM/GBSA: Strategies and Applications in Drug
734 Design. Chem Rev. 2019;119(16):9478-508. Epub 2019/06/28. doi:
735 10.1021/acs.chemrev.9b00055. PubMed PMID: 31244000.
736 44. Humphrey W, Dalke A, Schulten K. VMD: visual molecular dynamics. J Mol Graph.
737 1996;14(1):33-8, 27-8. Epub 1996/02/01. doi: 10.1016/0263-7855(96)00018-5. PubMed
738 PMID: 8744570.
739 45. REED LJ, MUENCH H. A SIMPLE METHOD OF ESTIMATING FIFTY PER CENT
740 ENDPOINTS12. American Journal of Epidemiology. 1938;27(3):493-7. doi:
741 10.1093/oxfordjournals.aje.a118408.
742 46. Zhang M, Wang H, Foster ER, Nikolov ZL, Fernando SD, King MD. Binding behavior of
743 spike protein and receptor binding domain of the SARS-CoV-2 virus at different
744 environmental conditions. Sci Rep. 2022;12(1):789. Epub 2022/01/19. doi: 10.1038/s41598-
745 021-04673-y. PubMed PMID: 35039570; PubMed Central PMCID: PMCPMC8763896.
746

748 **Figure Legends:**

749

750 **Figure 1. Computational insights exploring the cross-reactive SARS-CoV-2 antibodies at**
751 **DENV-2 E protein:** (A) Sequence and structural organization of the DENV-2 E dimer (PDB
752 1OAN). (B) Overview of the computational pipeline. (C) The binding free energy in kcal/mol
753 of selected SARS-CoV-2 antibodies. The most likely complexes were generated using Protein-
754 protein dockings. (D) The interaction map of top three antibodies (CR3022: 6W7Y: violet,
755 S2E12 neutralizing antibody Fab fragment: 7K45: orange and DMAb 2196: 8D8R: magenta)
756 along with the native antibody of DENV-2 E as control (C8:4UTA: green). The residue-wise
757 zoom-out view is shown to highlight the critical residues mainly forming the interactions such
758 as H bonds and SBs. The DENV-2 antibody interactions are shown in green-colored residues
759 and SARS-CoV-2 antibody interactions are highlighted in the pink-colored residues. (E) The
760 matrix of critical residues involved in either establishing either H-bonds or in SBs along with
761 their occurrence. (F) The per-residue decomposition of top three antibodies indicating the
762 thermodynamic contributions of epitope residues. (G) The net binding energy between
763 identified antibodies and DENV-2 E which claims as potential in both cases. (H) The 3D
764 positioning of identified epitope residues at dimer of DENV. The residues which only interact
765 with SARS-CoV-2 antibodies are shown in cyan, the residues interacting with only DENV-2
766 antibody are shown in green color. The residues which are interacting with both DENV-2 E as
767 well as with SARS-CoV-2 RBD are shown in violet color. All the residues are rendered in
768 licorice and atom-wise C: cyan/green/violet, N: blue, O: red and S: yellow.

769

770 **Figure 2: Cross-reactivity and ADE of Dengue virus infection by the SARS-CoV-2 anti-**
771 **RBD antibody CR3022.**

772 (A) Confocal, digital images of DENV-2 (NGC) infected C6/36 cells stained with CR3022
773 along with the controls, 4G2 and Rabishield® (taken from Figure 1 to show the comparison)
774 and the Mean Fluorescence Intensity (MFI).
775 (B) Binding kinetics of CR3022 with SARS-CoV-2 spike protein (i) and DENV-2 protein E
776 (ii).
777 (C) ADE of DENV-2 infection by different concentrations of CR3022 in K562 cells by
778 flowcytometry. Statistical significance was checked using One-way ANOVA followed by
779 Dunnett's test. Asterisk (*) indicates a statistically significant difference between the control
780 and treatment. P value = 0·1234 (ns), 0·0332 (*), 0·0021 (**), 0·0002 (***), <0·0001 (****).
781
782 **Figure 3: ADE of dengue virus infection by the SARS-CoV-2 positive patients' sera in**
783 **K562 cells.**
784 ADE due to convalescent plasma samples collected in the (A)first interval (Samples collected
785 from May 2020- Jan 2021), n=21, (B) second interval (Samples collected from May 2021-June
786 2021), n=17, and (C) third interval (Samples collected from Feb 2022-April 2022), n=10. The
787 bar graph represents an average percentage increase in DENV positive cells w.r.t. VC for each
788 sample with standard deviation for duplicates. Statistical significance was carried out using
789 One-way ANOVA followed by Dunnett's test in GraphPad Prism 8·4·2. Asterisk (*) indicates
790 that the difference between the virus control and the serum samples is statistically significant.
791 P value = 0·1234 (ns), 0·0332 (*), 0·0021 (**), 0·0002 (***), <0·0001 (****)
792 (D) Representative dot plots of patient samples from the first interval (#143, #155), second
793 interval (#96), and third interval (#2, #7). Data was analyzed on FlowJo version 10·8·1.
794
795 **Figure 4: Effect of SARS-CoV-2 on dengue infection in AG129 mice:** (A) Schematic
796 experimental plan showing three animal groups: Mock as G1, adeno-ACE-2 viral vector

797 infection at 5 days prior to day 0 in G2 and G3, SARS-CoV-2 infection at day 2 followed by
798 infection with Dengue virus at day 21 in G2, and dengue virus infection at day 21 in G3. (B)
799 Change in body weight. Two-way ANOVA was used. (C) SARS-CoV-2 Spike antibody
800 response at day 21 (D) DENV2 viral particles were quantified by FFU assay in the serum of
801 infected mice. To compare the two independent groups, the Mann-Whitney U test was applied
802 for the statistical analysis. (E-F) The DENV2 genome was quantified by qRT-PCR from 100mg
803 spleen and liver tissue. Based on the small sample size and comparing the two groups the
804 Student T-test was applied and data are represented as mean ± SEM, *P<0.05, **P<0.01. (G)
805 platelet count, (H) WBC count, (I) haematocrit percentages were measured. Data are
806 represented as mean ± SEM. *P < 0.05, **P < 0.01, ***P < 0.001, ****P < 0.0001, ns = non-
807 significant.
808
809 **Figure 5: Cross-reactivity of antibodies and sera raised against SARS-CoV-2 Spike with**
810 **DENV-2 (NGC) proteins.**
811 (A) Confocal, digital images of DENV-2 (NGC) infected C6/36 cells reacted with 4G2,
812 antibodies and sera raised against SARS-CoV-2 after 48 hpi. Cell nuclei are stained with DAPI
813 while the other antibodies are detected using FITC-labeled respective secondary antibodies.
814 (B) Bar graph showing MFI of 4G2, MSer, 1A9, P1R (normalized w.r.t. the respective
815 secondary antibody controls) with standard deviation. Analysis was performed using ImageJ
816 and statistical significance was carried out using One-way ANOVA followed by Dunnett's test
817 in GraphPad Prism 8·4·2. Asterisk (*) indicates statistically significant difference in MFI w.r.t.
818 Rabishield® (Negative control). P value = 0·1234 (ns), 0·0332 (*), 0·0021 (**), 0·0002 (***),
819 <0·0001 (****)
820 (C) Binding kinetics of C8 (DENV-E protein specific) and 1A9 (SARS-CoV-2 spike specific)
821 antibodies with DENV-2 protein E and SARS-CoV-2 spike protein. Antibodies were loaded

822 onto the sensors and serial dilutions of the proteins were used to study binding kinetics. The
823 binding responses were calculated by subtracting data from reference and fitting globally with
824 a 1:1 binding model using ForteBio's Data Analysis software 10·1. The data was considered
825 validated if $\chi 2 < 0{\cdot}5$.
826
827 **Figure 6: ADE of dengue virus infection by the monoclonal and polyclonal antibodies and**
828 **serum against SARS-CoV-2.**
829 ADE due to (A) anti-spike monoclonal antibodies, M1B, 1A9, and different volumes of MM41
830 (from 2 µl to 6 µl) and anti-spike polyclonal antibody raised in rabbit, P1R, (B) anti-RBD
831 monoclonal antibodies, M4B, and different volumes of M5B (from 2 µl to 6 µl), (C) hamster
832 serum immunized with SARS-CoV-2 spike and negative control (Rabishield®). Statistical
833 significance was calculated using One-way ANOVA followed by Dunnett's test in GraphPad
834 Prism 8·4·2. Asterisk (*) indicates that the difference between the virus control and the serum
835 samples is statistically significant. P value = 0·1234 (ns), 0·0332 (*), 0·0021 (**), 0·0002 (***),
836 <0·0001 (****).
837 (D) Representative dot plots. Data was analyzed using FlowJo version 10·8·1.
838
839
840
841

Figure 1

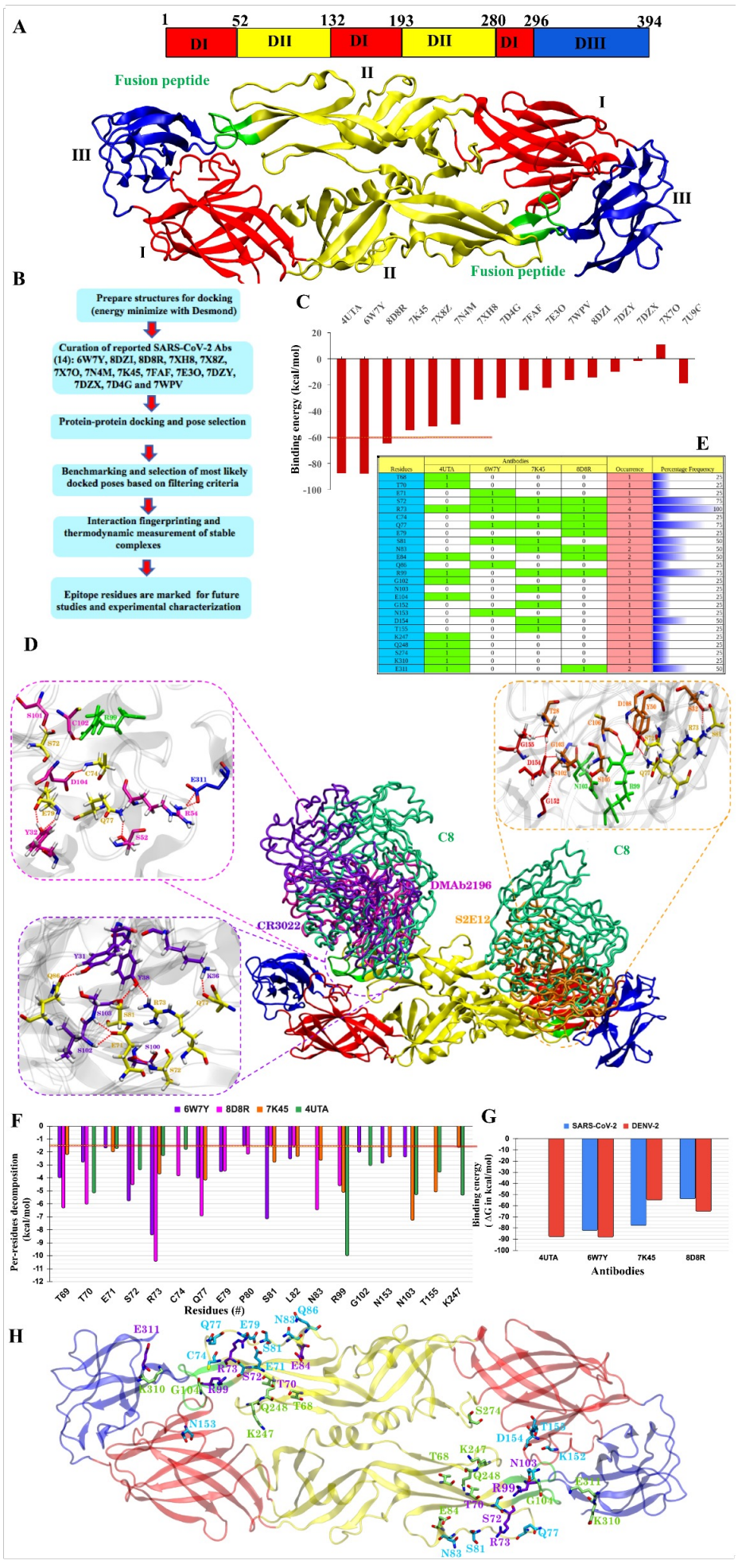

Residues	Antibodies				Occurrence	Percentage Frequency
	4UTA	6W7Y	7K45	8D8R		
T68	1	0	0	0	1	25
T70	1	0	0	0	1	25
E71	0	1	0	0	1	25
S72	0	1	1	1	3	75
R73	1	1	1	1	4	100
C74	0	0	0	1	1	25
Q77	0	1	1	1	3	75
E79	0	0	0	1	1	25
S81	0	1	1	0	2	50
N83	0	0	1	1	2	50
E84	1	0	0	1	2	50
Q86	0	1	0	0	1	25
R99	1	0	1	1	3	75
G102	1	0	0	0	1	25
N103	0	0	1	0	1	25
E104	1	0	0	0	1	25
G152	0	0	1	0	1	25
N153	0	1	0	0	1	25
D154	0	0	1	0	1	50
T155	0	0	1	0	1	25
K247	1	0	0	0	1	25
Q248	1	0	0	0	1	25
S274	1	0	0	0	1	25
K310	1	0	0	0	1	25
E311	1	0	0	1	2	50

Figure 2

A

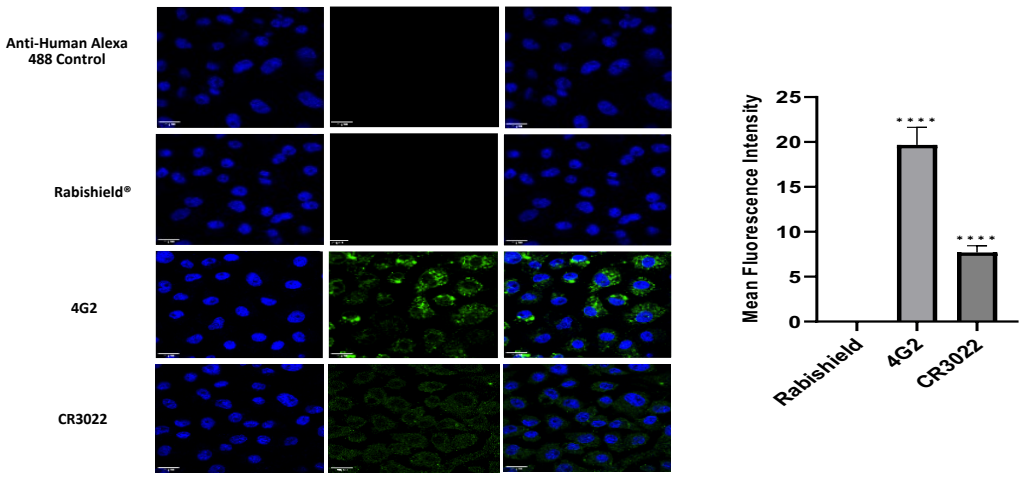
Anti-Human Alexa 488 Control
Rabishield®
4G2
CR3022
Mean Fluorescence Intensity
25
20
15
10
5
0
Rabishield
4G2
CR3022

B

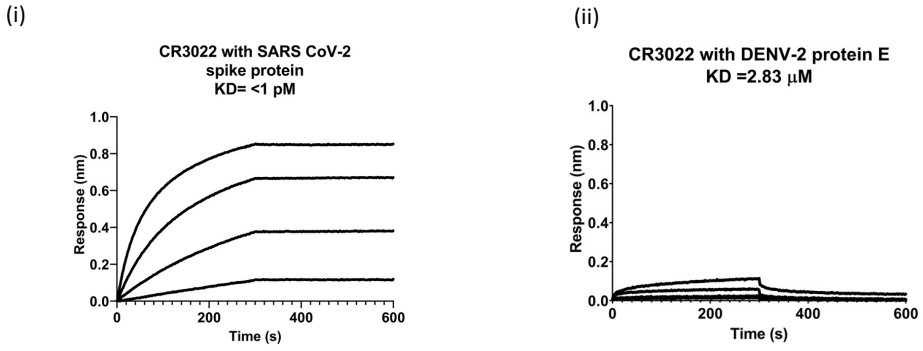
(i)
CR3022 with SARS CoV-2 spike protein
KD= <1 pM
Response (nm)
Time (s)
(ii)
CR3022 with DENV-2 protein E
KD =2.83 μM
Response (nm)
Time (s)

C

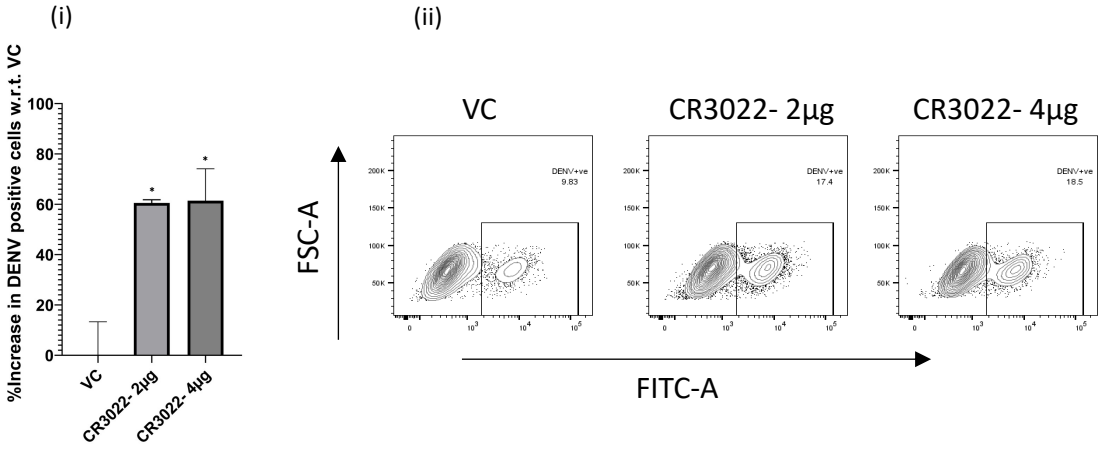
(i)
%Increase in DENV positive cells w.r.t. VC
VC
CR3022- 2μg
CR3022- 4μg
(ii)
VC
CR3022- 2μg
CR3022- 4μg
FSC-A
FITC-A

Figure 3

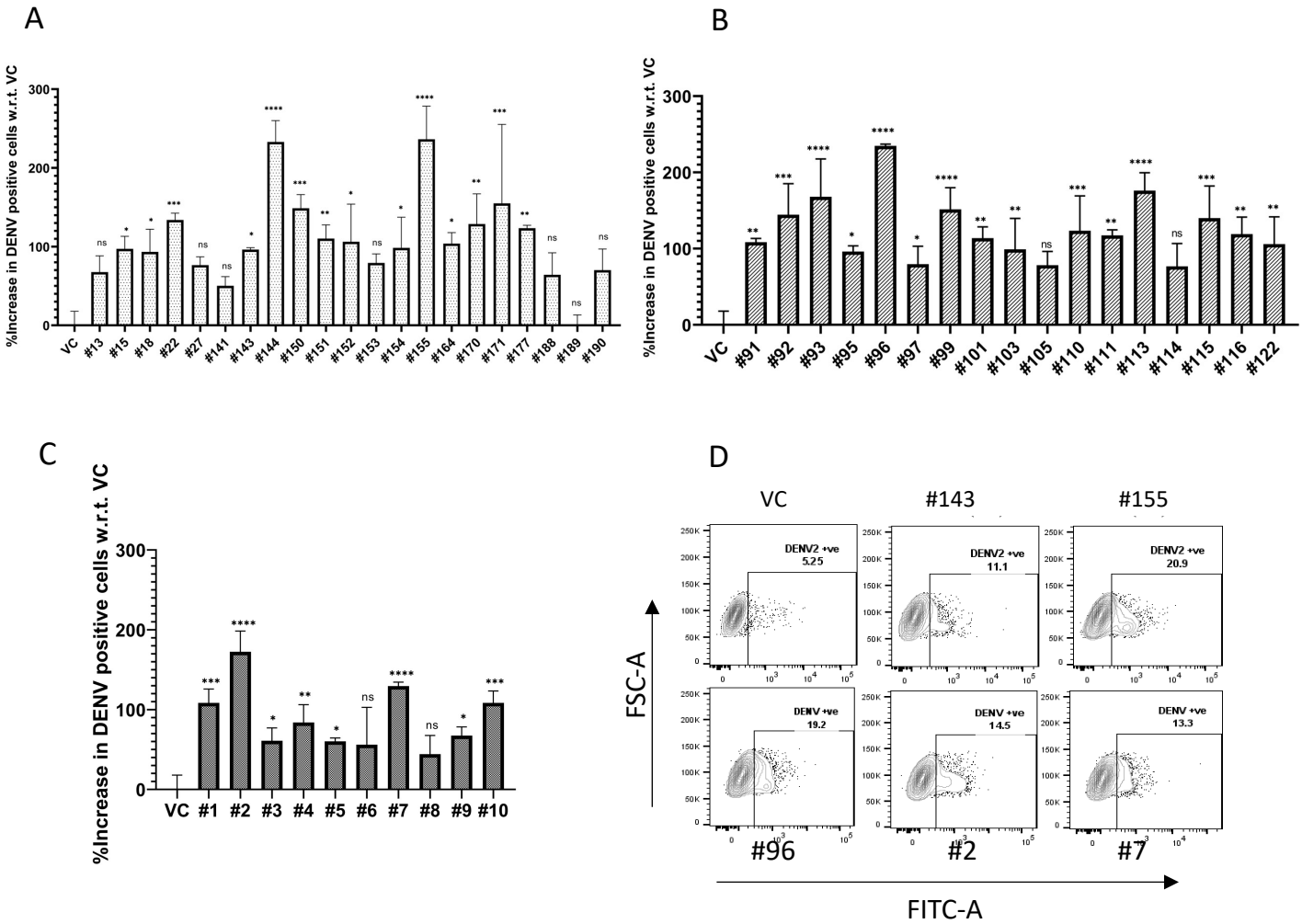
A
%Increase in DENV positive cells w.r.t. VC
300
200
100
0
VC
#13
#15
#18
#22
#27
#141
#143
#144
#150
#151
#152
#153
#154
#155
#164
#170
#171
#177
#188
#189
#190
B
%Increase in DENV positive cells w.r.t. VC
VC
#91
#92
#93
#95
#96
#97
#99
#101
#103
#105
#110
#111
#113
#114
#115
#116
#122
C
%Increase in DENV positive cells w.r.t. VC
VC
#1
#2
#3
#4
#5
#6
#7
#8
#9
#10
D
VC
#143
#155
DENV2 +ve
5.25
DENV2 +ve
11.1
DENV2 +ve
20.9
DENV +ve
19.2
DENV +ve
14.5
DENV +ve
13.3
#96
#2
#7
FSC-A
FITC-A

Figure 4

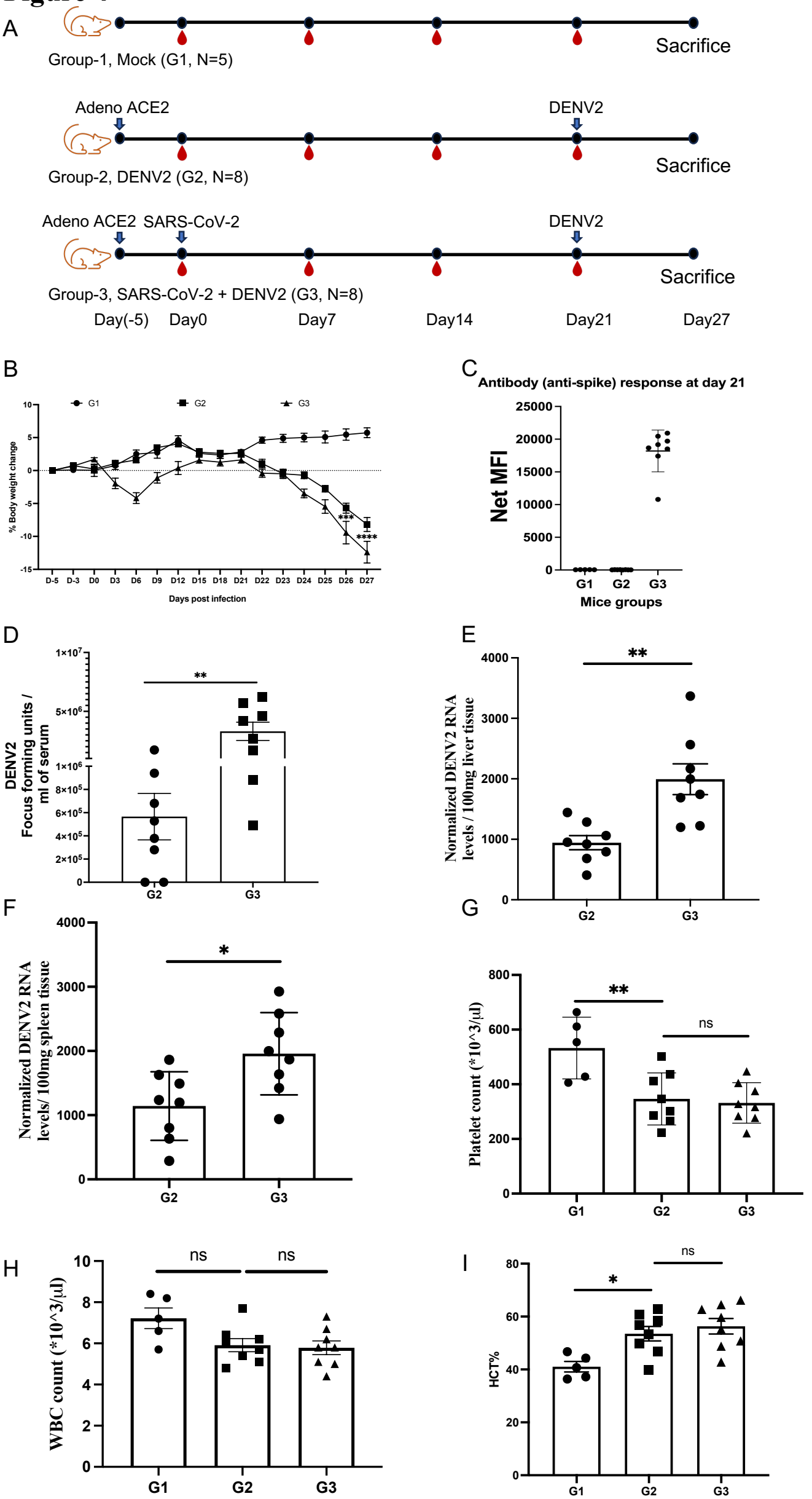
A
Group-1, Mock (G1, N=5)
Sacrifice
Adeno ACE2
DENV2
Group-2, DENV2 (G2, N=8)
Sacrifice
Adeno ACE2 SARS-CoV-2
DENV2
Group-3, SARS-CoV-2 + DENV2 (G3, N=8)
Sacrifice
Day(-5) Day0 Day7 Day14 Day21 Day27
B
G1 G2 G3
% Body weight change
Days post infection
C
Antibody (anti-spike) response at day 21
Net MFI
Mice groups
D
DENV2 Focus forming units / ml of serum
E
Normalized DENV2 RNA levels / 100mg liver tissue
F
Normalized DENV2 RNA levels/ 100mg spleen tissue
G
Platelet count (*10^3/µl)
H
WBC count (*10^3/µl)
I
HCT%

Figure 5

A

DAPI FITC Merged

Anti-mice Alexa 488 Control

4G2

Mser

1A9

MM41

Anti-Rabbit Alexa 488 Control

P1R

Anti-Human Alexa 488 Control

Rabishield®

B

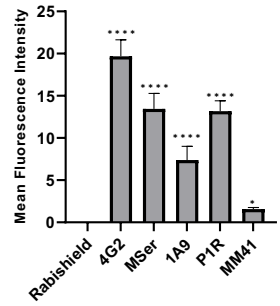

C

(i)

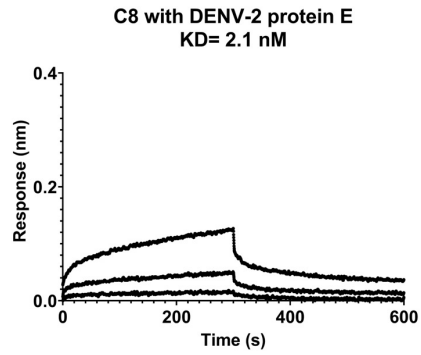

(ii)

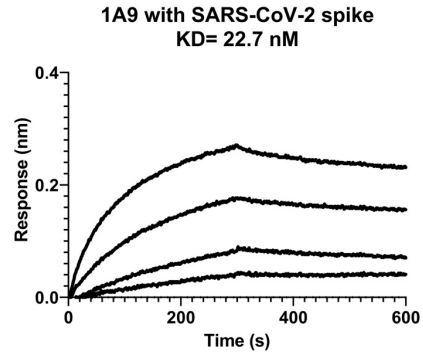

(iii)

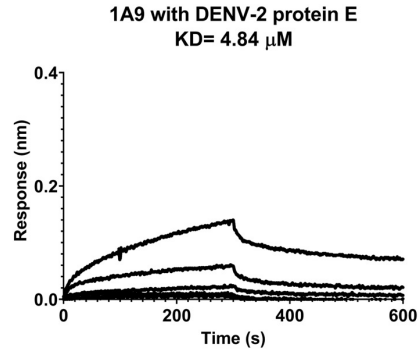

Figure 6

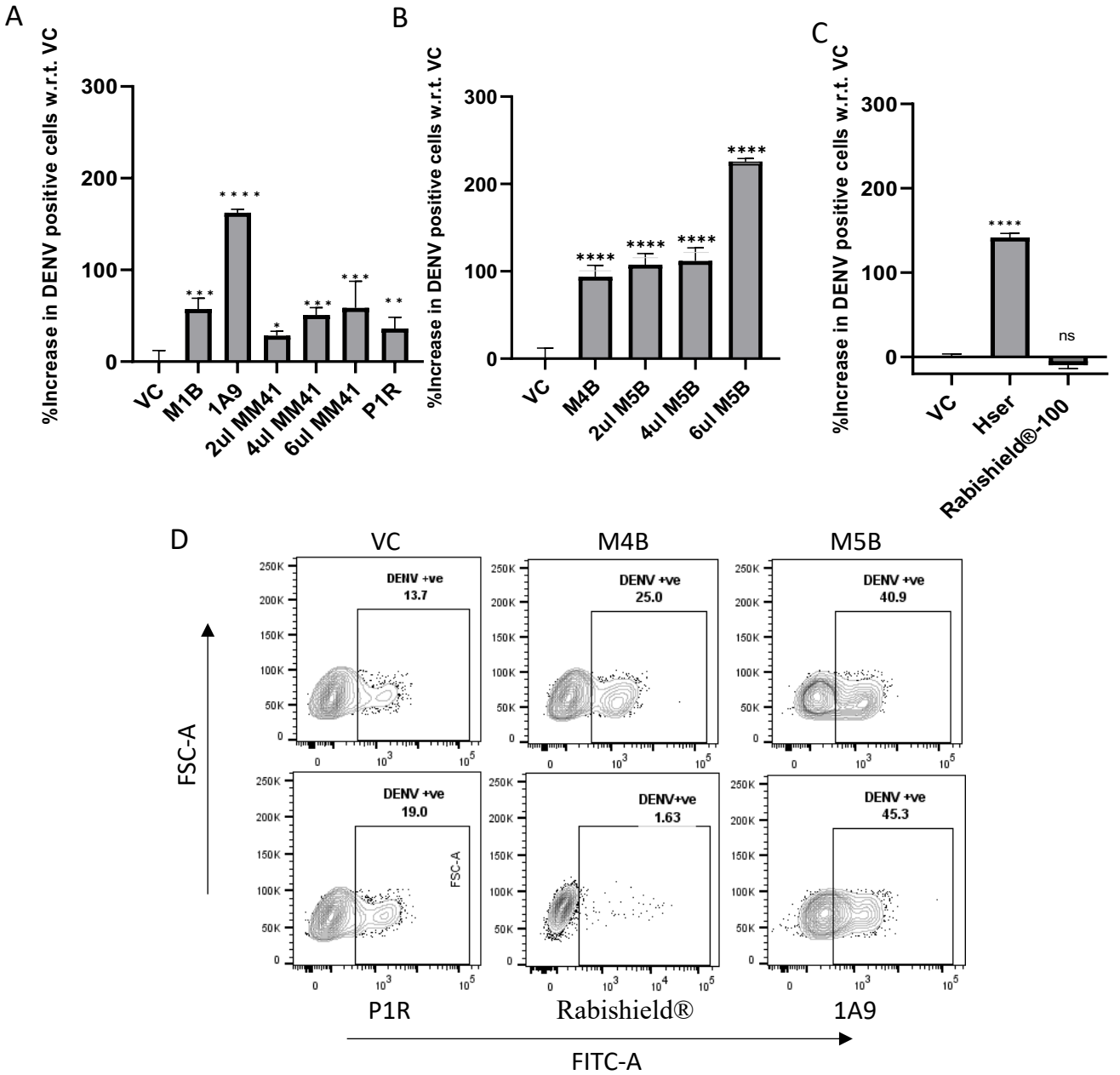
A
%Increase in DENV positive cells w.r.t. VC
300
200
100
0
VC
M1B
1A9
2ul MM41
4ul MM41
6ul MM41
P1R
B
%Increase in DENV positive cells w.r.t. VC
VC
M4B
2ul M5B
4ul M5B
6ul M5B
C
%Increase in DENV positive cells w.r.t. VC
ns
VC
Hser
Rabishield®-100
D
VC
M4B
M5B
DENV +ve 13.7
DENV +ve 25.0
DENV +ve 40.9
DENV +ve 19.0
DENV+ve 1.63
DENV +ve 45.3
FSC-A
P1R
Rabishield®
1A9
FITC-A